High-threshold fault-tolerant quantum computation with the Gottesman-Kitaev-Preskill qubit under noise in an optical setup

Kosuke Fukui

Department of Applied Physics, School of Engineering, The University of Tokyo, 7-3-1 Hongo, Bunkyo-ku, Tokyo 113-8656, Japan

(Received 13 February 2023; accepted 5 May 2023; published 22 May 2023)

To implement fault-tolerant quantum computation (FTQC) with continuous variables, continuous variables need to be digitized using an appropriate code such as the Gottesman-Kitaev-Preskill (GKP) qubit. The scheme introduced in [Fukui *et al.* Phys. Rev. X **8**, 021054 (2018)] has reduced the threshold of the squeezing level required for continuous-variable FTQC to less than 10 dB, assuming noise derived from the GKP qubit itself. In this paper, we propose a scheme to improve noise tolerance during the construction of a large-scale cluster state used for FTQC with the GKP qubits. In our scheme, a small-scale cluster state is prepared by employing maximum-likelihood estimation, the entanglement generation via the Bell measurement, and probabilistic reliable measurement. Then, a large-scale cluster state is constructed from the small-scale cluster states via the reliable encoded Bell measurement. In the numerical calculations, we assume errors derived from the two-mode gate and loss in the homodyne measurement in addition to noise from the GKP qubit itself. The results show that the thresholds of a squeezing level are around 8.1, 9.6, and 12.4 dB for loss in the homodyne measurement 0, 5, and 10%, respectively. Hence, this paper provides a way toward continuous-variable FTQC with a feasible squeezing level.

DOI: 10.1103/PhysRevA.107.052414

I. INTRODUCTION

Quantum computation (QC) has a great deal of potential to efficiently solve some hard problems for conventional computers [1,2]. To realize large-scale QC, a continuous-variable (CV) system is a promising platform [3–5]; in fact, larger-scale cluster states composed of the squeezed vacuum states have been experimentally generated in an optical setup [6–11]. Furthermore, thousands of frequency-encoded cluster states in an optical setup have been generated [12–15]. In addition to an optical setup, the continuous-variable (CV) system in a circuit QED [16], optomechanics [17,18], atomic ensembles [19,20], and a trapped ion mechanical oscillator [21,22] are also promising candidates for large-scale QC with CVs.

Towards fault-tolerant QC (FTQC) using CVs, it is known that CVs need to be encoded into appropriate bosonic codes [23–26], such as a cat code [27], a binomial code [28], or the Gottesman-Kitaev-Preskill (GKP) code [29], which is referred to as the GKP qubit in this paper. This is because the squeezed vacuum state cannot handle the accumulation of analog errors, such as those arising from the Gaussian quantum channel [29] and photon loss during QC. In 2014, Menicucci showed the threshold of the squeezing level for CV-FTQC [30], where the GKP qubit is used to perform the quantum error correction for measurement-based QC (MBQC). Recently, there have been many efforts towards CV-FTQC with the GKP qubit [31–50], and a promising architecture for a scalable quantum circuit incorporating the GKP qubit [51–53]. Furthermore, the GKP qubit is a promising element for a variety of quantum information processing such as long-distance quantum communication [54,55].

In Ref. [32], the required squeezing level for CV-FTQC has been alleviated to less than 10 dB, which is within the reach of the current experimental technology [56]. In an ion trap [22] and superconducting circuit quantum electrodynamics [57] the GKP qubit has been generated recently in an ion trap [22] and superconducting circuit quantum electrodynamics [57] with an achievable squeezing level close to 10 dB. In an optical setup, while there are many efforts to develop various ways to generate the GKP qubit [20,58–69], the optical GKP qubit has not been generated yet due to the difficulty to obtain a nonlinearity. Thus, there is a demand to reduce the experimental requirements to generate a sufficient GKP qubit for FTQC. In addition, the noise model in Ref. [32] assumes that the deviation is derived from the GKP qubit itself. Considering a practical optical setup, there are additional noises such as imperfections derived from the two-mode gate and the homodyne measurement. This leads to the degradation of the squeezing level threshold, which increases the requirements of CV-FTQC. For the aforementioned reasons, a further reduction of the threshold is needed for CV-FTQC in an optical setup.

In this paper, we propose a scheme to improve the required squeezing level for CV-FTQC under noise in the two-mode gate and the homodyne measurement. We develop a method to implement the highly reliable construction of the large-scale cluster state by harnessing the analog information contained

in the GKP qubits. Specifically, our method consists of two parts. One is to make use of the Gauss-Markov theorem, which is widely known in statistics. In this paper, we apply maximum-likelihood estimation to reduce the noise (displacement) of the GKP qubits in constructing the small-scale cluster state and use probabilistic operations to limit the accumulation of qubit-level errors. The other is the reliable deterministic entanglement generation to construct the large-scale cluster state from the small-scale cluster states. In this operation, we select the most reliable entanglement between node qubits by using a maximum-likelihood method, allowing us to safely remove the entanglements except for the most reliable one by employing the repetition code. Accordingly, the required squeezing level for CV-FTQC using the proposed method can be reduced to 8.1, 9.6, and 12.4 dB for the transmission loss in the homodyne measurement $l = 0, 5$, and 10 %, respectively, assuming the imperfection of the two-mode gate.

The rest of the paper is organized as follows. In Sec. II, we briefly review the background knowledge regarding the GKP qubit, and imperfections arising from the two-mode gate and the homodyne measurement. In Sec. III, we propose the method to reduce the required squeezing level for CV-FTQC with noise considered in this paper. In Sec. IV, the numerical results show an improvement in the threshold of the squeezing level compared to conventional methods. Section V is devoted to discussion and conclusion.

II. BACKGROUND

In this section, we first review the GKP qubits and noise model in this paper, assuming three noise sources, i.e., the deviation from the GKP qubit itself, the imperfection of the two-mode gate, and loss in the homodyne measurement [70]. Then, we describe two techniques used to improve noise tolerance with the GKP qubit: (1) the highly reliable measurement (HRM) and (2) the single-qubit level QEC with a maximum-likelihood estimation.

A. The GKP qubit

Gottesman, Kitaev, and Preskill proposed a method to encode a qubit in an oscillator's q (position) and p (momentum) quadratures to correct errors caused by a small deviation in the q and p quadratures [29]. We refer the state encoded by their scheme as the GKP qubit. The ideal code states of the GKP qubit are Dirac combs in the q and p quadratures [71]. The ideal 0 and 1 states are described as $|0\rangle_{\rm GKP} = \sum_{m=-\infty}^{\infty} |2m\sqrt{\pi}\rangle_q$ and $|1\rangle_{\rm GKP} = \sum_{m=-\infty}^{\infty} |(2m+1)\sqrt{\pi}\rangle_q$, respectively, where the eigenbasis of the position operator, $\{|x\rangle_q\}_{x\in\mathbb{R}}$, is conventionally used as the computational basis in CVs. The ideal GKP code state is not a normalizable state and it requires infinite squeezing. Thus, physical states for the GKP code are finitely squeezed approximations. The basis of the GKP qubit with finite squeezing is composed of a series of Gaussian peaks of width σ and separation $\sqrt{\pi}$ embedded in a larger Gaussian envelope of width $1/\sigma$. The approximate code states $|\widetilde{0}\rangle$ and $|\widetilde{1}\rangle$ are defined as

$$|\widetilde{0}\rangle \propto \sum_{t=-\infty}^{\infty} \int e^{-2\pi\sigma^2 t^2} e^{-(x-2t\sqrt{\pi})^2/(2\sigma^2)} |x\rangle_q \, dx, \tag{1}$$

$$|\widetilde{1}\rangle \propto \sum_{t=-\infty}^{\infty} \int e^{-\pi\sigma^2(2t+1)^2/2} e^{-(x-(2t+1)\sqrt{\pi})^2/(2\sigma^2)} |x\rangle_q \, dx. \tag{2}$$

The squeezing level s is defined by $s = -10\log_{10}(2\sigma^2)$. In the case of finite squeezing, there is a finite probability of misidentifying $|\widetilde{0}\rangle$ as $|\widetilde{1}\rangle$, and vice versa. Provided the magnitude of the true deviation is more than $\sqrt{\pi}/2$ from the peak value, the decision of the bit value is incorrect. The probability $E(\sigma^2)$ of misidentifying the bit value is calculated by

$$E(\sigma^2) = 1 - \int_{\frac{-\sqrt{\pi}}{2}}^{\frac{\sqrt{\pi}}{2}} dx \frac{1}{\sqrt{2\pi\sigma^2}} e^{-\frac{x^2}{2\sigma^2}}, \tag{3}$$

which corresponds to bit- or phase-flip errors on the GKP qubit. We mention that q and p quadratures are also referred to as Z and X bases, respectively.

We also describe the so-called qunaught state which is introduced in Ref. [72] for quantum sensing applications. The qunaught state $|\varnothing\rangle$ is described as

$$|\varnothing\rangle \propto \sum_{k=-\infty}^{\infty} e^{-i\sqrt{2\pi}k\hat{p}} |0\rangle_q = \sum_{k=-\infty}^{\infty} e^{i\sqrt{2\pi}k\hat{q}} |0\rangle_p, \tag{4}$$

where $\{|x\rangle_p\}_{x\in\mathbb{R}}$ is the eigenbasis of the momentum operator, which corresponds to the conjugate basis of $\{|x\rangle_q\}_{x\in\mathbb{R}}$. Two qunaught states are transformed to a Bell pair of the GKP qubits by a 50:50 beam-splitter coupling as $|\varnothing\rangle \otimes |\varnothing\rangle \mapsto (|\bar{0}\bar{0}\rangle + |\bar{1}\bar{1}\rangle)/\sqrt{2}$ [39].

In the case of the qunaught state with the variances σ^2 in both quadratures, the variances of each GKP qubit in the generated Bell pair are σ^2 in both quadratures. One advantage of employing the Bell pair from two qunaught states is error tolerance in terms of variances. Specifically, the variances of each GKP qubit in the entangled pair generated from the controlled-Z (CZ) gate between two GKP qubits are σ^2 and $2\sigma^2$ in the q and p quadratures, respectively. Thus, the error probability for the entangled pair from two qunaught states, instead of two GKP qubits, is smaller than that prepared from the two GKP qubits, where the error probability is obtained from Eq. (3). In this paper, we prepare the small-scale cluster state from qunaught states, as described in Sec. III A.

B. Noise in the two-mode gate

In this paper, we consider the optical quantum nondemolition (QND) gate as the two-mode gate between the GKP qubits, which has been demonstrated in Refs. [73,74]. In the QND gate, we prepare the two GKP qubits as data qubits and two squeezed vacuum states as ancillary states. Then, we implement a measurement-based two-mode gate where only the ancillary states are measured, i.e., the data qubits are not destroyed. For noise in the two-mode gate in this paper, we consider noise from the ancilla squeezed vacuum states.

For the optical QND gate via the squeezed vacuum state, two GKP qubits and two squeezed vacuum states interfere in the beam splitter with a transmittance coefficient $\sqrt{R}$, and

their quadrature operators transform as

$$\hat{q}_C \to \hat{q}_C - \sqrt{\frac{1-R}{1+R}}\hat{q}_A e^{-r_A}, \tag{5}$$

$$\hat{p}_C \to \hat{p}_C - \frac{1-R}{\sqrt{R}}\hat{p}_T + \sqrt{\frac{R(1-R)}{1+R}}\hat{p}_B e^{-r_B}, \tag{6}$$

$$\hat{q}_T \to \frac{1-R}{\sqrt{R}}\hat{q}_C + \hat{q}_T + \sqrt{\frac{R(1-R)}{1+R}}\hat{q}_A e^{-r_A}, \tag{7}$$

$$\hat{p}_T \to \hat{p}_T + \sqrt{\frac{1-R}{1+R}}\hat{p}_B e^{-r_B}, \tag{8}$$

where $\hat{q}_C(\hat{p}_C)$, $\hat{q}_T(\hat{p}_T)$, $\hat{q}_A(\hat{p}_A)$, and $\hat{q}_B(\hat{p}_B)$ are the quadrature operators of the control qubit, target qubit, and two squeezed vacuum states in the q (p), respectively, and r_A (r_B) is the squeezing parameter for the ancillary state A (B). In the case that the coefficient $(1-R)/\sqrt{R}$ is equal to 1 and the squeezing level of ancillary squeezed vacuum states is infinite, the QND gate is equivalent to the ideal controlled-X (CX) gate, which corresponds to the operator $\exp(-i\hat{q}_C\hat{p}_T)$. For the controlled-$Z$ (CZ) gate, the QND gate is equivalent to the CZ gate up to local Fourier transformations.

Regarding the variance of the GKP qubit, the QND gate changes the variances of the control and target qubits as

$$\sigma^2_{C,q} \to \sigma^2_{C,q} + \frac{1-R}{1+R}\sigma^2_A, \tag{9}$$

$$\sigma^2_{C,p} \to \sigma^2_{C,p} + \frac{(1-R)^2}{R}\sigma^2_{C,p} + \frac{R(1-R)}{1+R}\sigma^2_B, \tag{10}$$

$$\sigma^2_{T,q} \to \sigma^2_{C,q} + \frac{(1-R)^2}{R}\sigma^2_{T,q} + \frac{R(1-R)}{1+R}\sigma^2_A, \tag{11}$$

$$\sigma^2_{T,p} \to \sigma^2_{T,p} + \frac{1-R}{1+R}\sigma^2_B, \tag{12}$$

where $\sigma^2_{C,q(p)}$ and $\sigma^2_{T,q(p)}$ are the variances of the control qubit and the target qubit in the $q(p)$ quadrature, respectively, and $\sigma^2_{A(B)} = \frac{1}{2}e^{-2r_{A(B)}}$ is the variance of the ancillary state A (B). In this paper, we consider the increase in variances due to the squeezed vacuum states as noise in the two-mode gate, assuming that $\sigma^2_A = \sigma^2_B$. Additionally, we set a squeezing level of the ancillary squeezed vacuum to 15 dB in numerical calculations, a squeezing level that has been successfully achieved in the experimental setup reported in Ref. [75].

C. Photon loss in the homodyne measurement

Secondly, we consider the effects of photon loss in the homodyne measurement, which can be modeled as a beam-splitter coupling between the data qubit and a vacuum state, resulting in additional noise. The beam-splitter coupling transforms the quadrature operators for the data qubit in the q and p quadratures as

$$\hat{q} \to \sqrt{\eta}\hat{q} + \sqrt{1-\eta}\hat{q}_{\rm vac}, \tag{13}$$

$$\hat{p} \to \sqrt{\eta}\hat{p} + \sqrt{1-\eta}\hat{p}_{\rm vac}, \tag{14}$$

respectively, where $\sqrt{\eta}$ represents the transmittance coefficient for the beam-splitter coupling, and $\hat{q}_{\rm vac}$ ($\hat{p}_{\rm vac}$) denotes the operator for the vacuum state in the $q(p)$ quadrature. The variance of the input state in the $q(p)$ quadrature, $\sigma^2{}_{{\rm in},q(p)}$, changes as

$$\sigma^2{}_{{\rm in},q(p)} \to \sigma^2_{{\rm out},q(p)} = \eta\sigma^2_{{\rm in},q(p)} + \frac{1-\eta}{2}. \tag{15}$$

In the measurement after loss, the outcome from the homodyne measurement is multiplied by $1/\sqrt{\eta}$ in classical postprocessing since the peaks of the GKP qubit are fixed at integer multiples of $\sqrt{\pi}$ due to the GKP codewords. Consequently, the probability to misidentify the bit value in the $q(p)$ quadrature is calculated by $E(\sigma^{2\prime}{}_{{\rm out},q(p)})$ using Eq. (3), where $\sigma^{2\prime}{}_{{\rm out},q(p)}$ is given by

$$\sigma^{2\prime}{}_{{\rm out},q(p)} = \frac{\sigma^2_{{\rm out},q(p)}}{\eta} = \sigma^2_{{\rm in},q(p)} + \frac{1-\eta}{2\eta}. \tag{16}$$

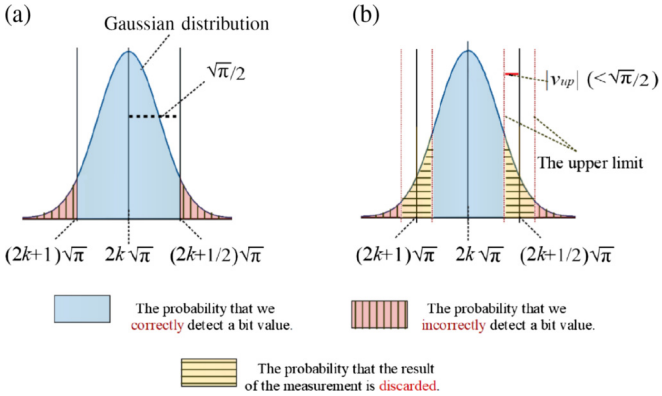

FIG. 1. Introduction of the highly reliable measurement. (a) The conventional measurement of the GKP qubit, where the Gaussian distribution is followed by the deviation of the GKP qubit whose variance is σ^2. The plain (blue) region and the region with the vertical (red) line represent the different code words $(k-1)$ mod 2 and $(k+1)$ mod 2, respectively. The vertical line regions correspond to the probability of incorrect decision of the bit value. (b) The highly reliable measurement. The shown dot line represents an upper limit $v_{\rm up}$. The horizontal areas show the probabilities of measurement results being discarded upon the introduction of $v_{\rm up}$. The vertical line areas show the probability that our method fails.

D. Highly reliable measurement

The HRM reduces the probability of misidentifying the bit value of the GKP qubit by introducing upper limit $v_{\rm up}$ as a decision line of the bit value, as shown in Fig. 1(a). In the conventional measurement, the decision sets an upper limit for $|\Delta_m|$ at $\sqrt{\pi}/2$, and assigns the bit value $k = (2t+k)\sqrt{\pi}$. In the HRM, the decision sets an upper limit at $v_{\rm up}(<\sqrt{\pi}/2)$ to give the maximum deviation that will not cause incorrect measurement of the bit value as shown in Fig. 1. If the above condition $|\Delta_m| < v_{\rm up}$ is not satisfied, we discard the result. Since the measurement error occurs when $|\bar{\Delta}|$ exceeds $|\sqrt{\pi}/2 + v_{\rm up}|$, the error probability decreases with increasing $v_{\rm up}$ at the cost of the success probability of the measurement. The probability of misidentifying the bit value with the HRM for the variance σ^2 is given by

$$E_{v_{\rm up}}(\sigma^2) = \frac{P^{\rm in}_{v_{\rm up}}(\sigma^2)}{P^{\rm cor}_{v_{\rm up}}(\sigma^2) + P^{\rm in}_{v_{\rm up}}(\sigma^2)}, \tag{17}$$

where $P^{\rm cor}_{v_{\rm up}}(\sigma^2)$ is the probability that the true deviation $|\bar{\Delta}|$ falls in the correct area, and $P^{\rm in}_{v_{\rm up}}(\sigma^2)$ is the probability that the true deviation $|\bar{\Delta}|$ falls in the incorrect area. The probabilities, $P^{\rm cor}_{v_{\rm up}}(\sigma^2)$ and $P^{\rm in}_{v_{\rm up}}(\sigma^2)$, are given by

$$P^{\rm cor}_{v_{\rm up}} = \sum_{k=-\infty}^{+\infty} \int_{2k\sqrt{\pi}-\frac{\sqrt{\pi}}{2}+v_{\rm up}}^{2k\sqrt{\pi}+\frac{\sqrt{\pi}}{2}-v_{\rm up}} dx \frac{1}{\sqrt{2\pi\sigma^2}} e^{-\frac{x^2}{2\sigma^2}} \tag{18}$$

and

$$P^{\rm in}_{v_{\rm up}} = \sum_{k=-\infty}^{+\infty} \int_{(2k+1)\sqrt{\pi}-\frac{\sqrt{\pi}}{2}+v_{\rm up}}^{(2k+1)\sqrt{\pi}+\frac{\sqrt{\pi}}{2}-v_{\rm up}} dx \frac{1}{\sqrt{2\pi\sigma^2}} e^{-\frac{x^2}{2\sigma^2}}, \tag{19}$$

respectively.

E. The SQEC with a maximum-likelihood estimation

In this subsection, we describe the single-qubit level QEC (SQEC) and propose the SQEC with a maximum-likelihood estimation (ME-SQEC). The SQEC is used to correct small displacement (deviation) errors in both quadratures, while it cannot correct bit- and phase-flip errors [29]. We describe the SQEC in the q quadrature, assuming ideal two-mode gates here (see also Appendix A for the SQEC in the p quadrature). To correct the small deviation of the data qubit D in the q quadrature, the ancilla qubit A is prepared in the logical state $|\widetilde{+}\rangle_A$, and is entangled with the data qubit using the ideal CX gate, with the data and ancilla qubits serving as the target and control qubits, respectively. The ideal CX gate described by $\exp(-i\hat{q}_{\rm a}\hat{p}_D)$ transforms the deviation values of data and ancilla qubits as

$$\overline{\Delta}_{q,a} \to \overline{\Delta}_{q,a} + \overline{\Delta}_{q,D}, \tag{20}$$

$$\overline{\Delta}_{p,a} \to \overline{\Delta}_{p,a}, \tag{21}$$

$$\overline{\Delta}_{q,D} \to \overline{\Delta}_{q,D}, \tag{22}$$

$$\overline{\Delta}_{p,D} \to \overline{\Delta}_{p,D} - \overline{\Delta}_{p,a}, \tag{23}$$

where $\overline{\Delta}_{q,D}(\overline{\Delta}_{p,D})$ and $\overline{\Delta}_{q,a}(\overline{\Delta}_{p,a})$ are the true deviation values of the data and ancilla qubits in the q (p) quadrature, respectively. Then, we measure the ancilla qubit in the q quadrature and obtain the measurement outcome $m_{q,m} = (2t+k)\sqrt{\pi} + \Delta_{mq,a}$ to minimize $|\Delta_{mq,a}|$, where k is the bit value and $t = 0, \pm1, \pm2, \ldots$. Then, we perform the displacement operation on the data qubit in the q quadrature by the measured deviation $\Delta_{mq,a}$. If $|\overline{\Delta}_{q,a} + \overline{\Delta}_{q,D}|$ is less than $\sqrt{\pi}/2$, the true deviation value of the data qubit in the q quadrature changes to $-\overline{\Delta}_{q,a}$, where the deviation of the data qubit, $\overline{\Delta}_{q,D}$, is displaced by the measured deviation $\overline{\Delta}_{q,a} + \overline{\Delta}_{q,D}$. On the other hand, if $|\overline{\Delta}_{q,a} + \overline{\Delta}_{q,D}|$ is more than $\sqrt{\pi}/2$, the bit-flip error occurs. Using Eq. (3), we obtain the error probability of the bit-flip error as $E(\sigma^2_{D,q} + \sigma^2_{a,q})$, assuming that the variances of the data (ancilla) qubit in the q and p quadratures are $\sigma^2_{D(a),q}$ and $\sigma^2_{D(a),p}$, respectively. As a consequence, the SQEC in the q quadrature reduces the variance of the data qubit in the q quadrature from $\sigma^2_{D,q}$ to $\sigma^2_{a,q}$, when $\sigma^2_{D,q} > \sigma^2_{a,q}$. Regarding the variance of the data qubit in the p quadrature, the SQEC increases the variance from $\sigma^2_{D,p}$ to $\sigma^2_{D,p} + \sigma^2_{a,p}$.

In this paper, we introduce the ME-SQEC to improve noise tolerance. In the ME-SQEC, we estimate the true deviation of the data qubit by considering the Gauss-Markov theorem. The Gauss-Markov theorem is widely known in statistics and asserts that the ordinary least-squares estimator in the linear regression model is the best linear unbiased estimator under specific conditions [76]. Here, we describe the ME-SQEC in the q quadrature, where we perform the CZ gate between the data qubit and ancilla qubit, followed by measuring the ancilla qubit. Considering the least-squares method, the true deviation of the GKP qubit follows the posterior probability corresponding to Gaussian distribution of mean δ and the variance $\sigma'^2_{q,D}$, where δ and $\sigma'^2_{q,D}$ are given by

$$\delta = \frac{\sigma^2_{q,D}}{\sigma^2_{q,D} + \sigma^2_{p,A}} (\overline{\Delta}_{p,A} - \overline{\Delta}_{q,D}) \tag{24}$$

and

$$\sigma'^2_{q,D} = \frac{\sigma^2_{q,D}\sigma^2_{p,A}}{\sigma^2_{q,D} + \sigma^2_{p,A}}, \tag{25}$$

respectively. We note that the proposed maximum-likelihood estimation is based on the fact that the true deviation values follow a Gaussian distribution independently. Then, by performing the displacement operation on the data qubit by δ, the variance of the qubit D in the q quadrature decreases from $\sigma^2_{p,A}$ to $\sigma'^2_{q,D}$, while the variance in the p quadrature increases from $\sigma^2_{p,D}$ to $\sigma^2_{p,D} + \sigma^2_{q,A}$. In the case where $\sigma^2_{p,D} = \sigma^2_{q,A} = \sigma^2$, the ME-SQEC improves the variance of the data qubit in the q quadrature by $\sigma^2/2$ in comparison to the SQEC without a maximum-likelihood estimation. In the measurement, qubit-level errors occur when the deviation value is more than $\sqrt{\pi}/2$ and the misidentification of the bit value occurs. To reduce the probability of misidentifying the ancilla's bit value, we use the HRM during the construction of the small-scale cluster state, as described in the next section.

III. HIGHLY RELIABLE LARGE-SCALE CLUSTER STATE CONSTRUCTION

In this section, we introduce the scheme for applying the ME-SQEC to the construction of a small-scale cluster state. Then, we describe the construction of a large-scale cluster state from the small-scale cluster states, where the repetition code with the analog QEC is employed to reduce measurement errors.

A. Small-scale cluster state construction

In this paper, we prepare the small-scale cluster states from the qunaught states and the GKP qubits using HRM and ME-SQEC. Figure 2 shows the schematic diagram of the proposed scheme for preparing reliable small-scale cluster states, where larger-scale cluster states are generated from smaller-scale cluster states via the fusion gate and the two-mode gate with HRM. In this subsection, we describe the construction of two types of five-tree cluster states described in Figs. 2(g) and 2(h), which are used to construct larger-scale cluster states with HRM.

First, we prepare two types of two-mode entangled pairs: the balanced-entangled pair and the biased-entangled pair. For the balanced-entangled pair, the Bell pair of GKP qubits

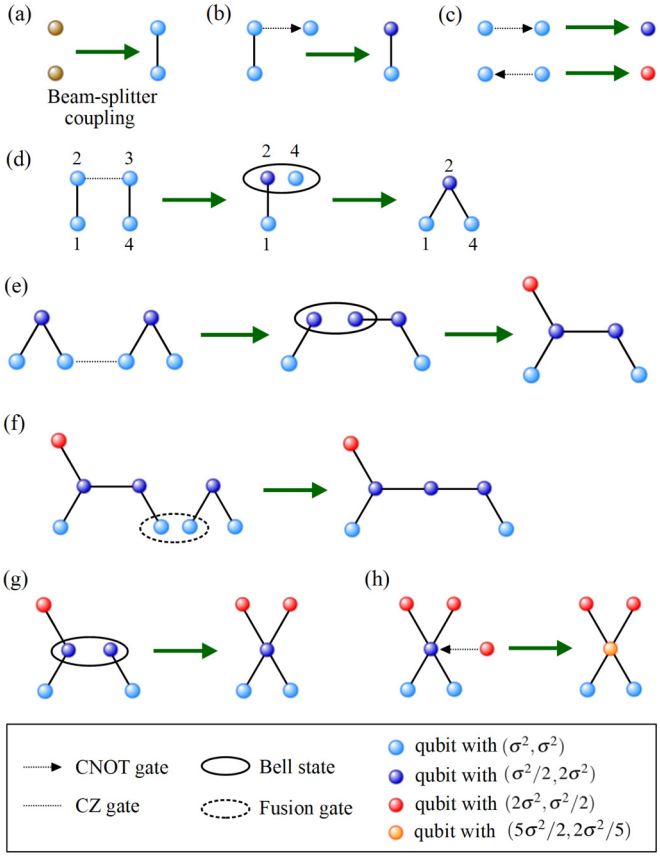

FIG. 2. The preparation of small-scale cluster states with the ME-SQEC and the highly reliable measurement (HRM). (a) The generation of the balanced-entangled pair of two GKP qubits via 50:50 beam-splitter coupling between two qunaught states. (b) The generation of the biased-single qubits via the ME-SQEC. (c) The generation of the biased-entangled pair via the ME-SQEC in the p quadrature on one of the biased-entangled pairs in Fig. 2(b), where the ancilla qubit is prepared in $|\widetilde{0}\rangle$ as the control qubit for the CNOT gate. (d) The generation of the three-tree cluster state from the two balanced-entangled pairs. (e) The construction of the five-mode cluster state from the two three-tree cluster states. (f) The construction of the six-mode cluster state from the five-mode cluster state and the three-tree cluster state. (g), (h) The construction of two types of five-tree cluster states.

is generated using a 50:50 beam splitter between the two qunaught states, as shown in Fig. 2(a), where the qunaught state, $|\varnothing\rangle$, is described in Sec. II A. For simplicity, we assume that the two-mode gate for the ME-SQEC is ideal in this section. For the variances, each GKP qubit of the entangled state has variances of (σ^2,σ^2), i.e., variances in the q and p quadratures are both σ^2. After the Fourier transformation on one of the qubits, we obtain the two-mode cluster state. For the biased-entangled pairs, the ME-SQEC with the HRM in the q quadrature is applied to one of the entangled pairs, as shown in Fig. 2(b), where the variances are transformed from (σ^2,σ^2) to $(\sigma^2/2,2\sigma^2)$ [77]. Figure 2(c) shows the preparation of the biased-single qubit via the ME-SQECs in the q and p quadratures, where the variances are transformed from (σ^2,σ^2) to $(\sigma^2/2,2\sigma^2)$ and $(2\sigma^2,\sigma^2/2)$, respectively. The two biased-single qubits are used for the ME-SQECs on the qubit whose variance is not (σ^2,σ^2).

Then, we generate the three-tree cluster states via the CZ gate between each qubit of the two balanced-entangled pairs, as shown in Fig. 2(d). Considering the variances of the GKP qubits in the balanced-entangled pair, the CZ gate transforms the variances of qubits 2 and 3 from (σ^2,σ^2) to $(\sigma^2,2\sigma^2)$. After measuring qubit 3, qubits 2 and 4 are entangled as the Bell state. After performing Fourier transformation on qubit 4, the three-tree cluster state is prepared. The variances for qubits 1 and 4 and for qubit 3 are (σ^2,σ^2) and $(\sigma^2/2,2\sigma^2)$, respectively. We note that the ME-SQEC is employed after the measurement of qubit 3 to reduce the variance in the q quadrature. Figure 2(e) shows the construction of the five-mode cluster state, where the two three-tree cluster states are entangled by the CZ gate and one of the qubits is measured. In the measurement, the ME-SQEC with the HRM is employed on the qubit whose variances are transformed as $(\sigma^2,\sigma^2)\mapsto(\sigma^2/2,2\sigma^2)$. After the Fourier transformation, the five-mode cluster state is prepared, where the Fourier transformation transforms variances from $(\sigma^2/2,2\sigma^2)$ to $(2\sigma^2,2\sigma^2/2)$. Figure 2(f) shows the construction of the six-mode cluster state from the five-mode cluster state and the three-tree cluster state via the Bell measurement. We refer to the entanglement generation via the Bell measurement as the fusion gate.

Then, we prepare two types of five-tree cluster states, as shown in Figs. 2(g) and 2(h). The five-tree cluster state in Fig. 2(g) is prepared by the measurement of one of the qubits in the six-mode cluster state and the Fourier transformation. We note that the error probability in the measurement during the construction of the cluster states in Figs. 2(d)–2(g) is given by $E_{v_{\rm up}}(2\sigma^2)$. The five-tree cluster state in Fig. 2(h) is prepared by employing the ME-SQEC in the p quadrature between the two qubits in the five-tree cluster state in Fig. 2(g) and the biased-single qubit in Fig. 2(c). This ME-SQEC transforms the variances from $(\sigma^2/2,2\sigma^2)$ to $(5\sigma^2/2,2\sigma^2/5)$. The error probability in this ME-SQEC is given by $E_{v_{\rm up}}(5\sigma^2/2)$. After preparing the small-scale cluster states described in Fig. 2, we construct the encoded hexagonal cluster state. Figure 3(a) shows the encoded hexagonal cluster state, where each of the six node qubits is connected to two encoded leaf qubits. Each encoded leaf qubit consists of the encoded ancilla qubits, and each encoded ancilla qubit consists of the single leaf qubit and three ancilla qubits. The procedure for generating such small-scale cluster states is similar to the one introduced in Ref. [32]. The details for the construction of the encoded hexagonal cluster are described in Appendix B. In the construction of the hexagonal cluster state, the maximum error probability for the fusion gate with the proposed scheme is $E_{v_{\rm up}}(5\sigma^2/2)$, while with the conventional scheme [32] it is $E_{v_{\rm up}}(3\sigma^2)$. Additionally, the error probabilities for the ME-SQECs during the construction of small-scale cluster states are limited to $E_{v_{\rm up}}(5\sigma^2/2)$ at most. Consequently, we obtain the three-tree cluster state with low error accumulation.

B. Large-scale cluster state construction with the encoded measurement

After preparing the encoded hexagonal cluster states, we construct the so-called Raussendorf-Harrington-Goyal lattice

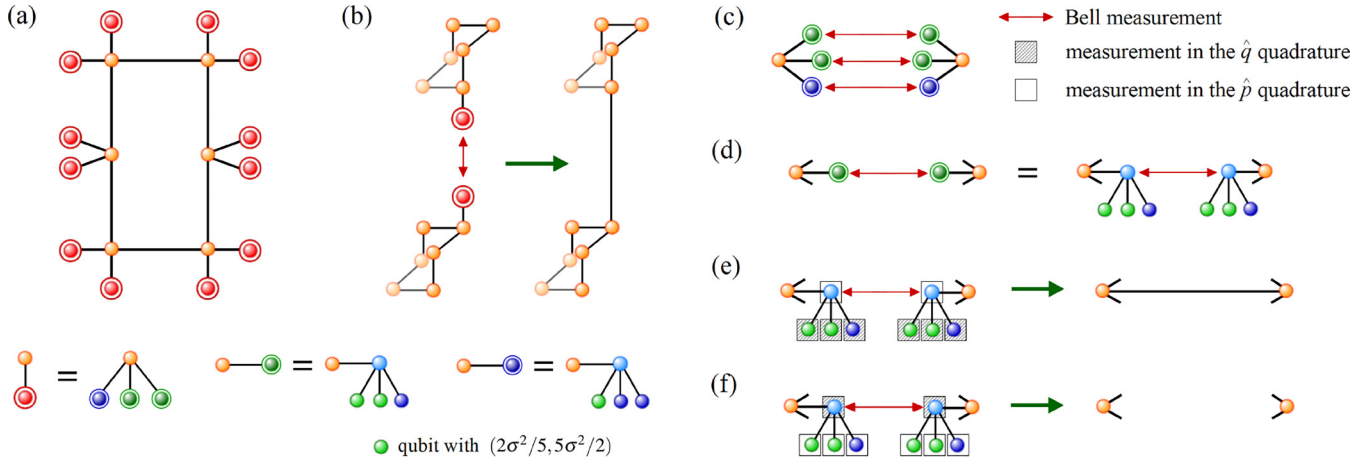

FIG. 3. The construction of a large 3D cluster state. (a) The hexagonal cluster state with the encoded leaf qubits, where each of six node qubits is entangled with $2L$ encoded leaf qubits and two neighboring node qubits. Each encoded leaf qubit consists of a single leaf qubit and m ancilla qubits. (b) The encoded Bell measurement between the two encoded leaf qubits in the neighboring hexagonal cluster states. (c) The m-Bell measurements for each encoded Bell measurement. (d) Each measurement of the m Bell measurements between the two neighboring qubits. (e) The measurement on the ancillae in the q quadrature to keep the most reliable entanglement by comparing the reliabilities obtained from the measurement results of the Bell measurement. (f) The measurement on the ancillae in the p quadrature to discard the entanglement except for the most reliable entanglement, which corresponds to the encoded measurement with the m-repetition code in the q quadrature.

referred to as the three-dimensional (3D) cluster state in this paper. In this step, the large-scale 3D cluster state must be constructed deterministically from the encoded hexagonal cluster states since large-scale QC should be implemented deterministically. In Ref. [32], the large-scale 3D cluster state is constructed from the hexagonal cluster described by using the deterministic fusion gate without the HRM. The bottleneck to improve the threshold of squeezing level, as obtained in Ref. [32], is the error arising from the deterministic fusion gate since the error probability of the deterministic fusion gate is several orders of magnitude higher than that of the fusion gate with the HRM. In this paper, we employ the encoded hexagonal cluster state to reduce the error probability of the deterministic fusion gate by using encoded ancilla qubits, as shown in Fig. 3(b). Consequently, we can perform topologically protected MBQC on the highly reliable 3D cluster state.

Here we describe the fusion gate with the encoded measurement in more detail, which realizes deterministic and reliable entanglement generation between neighboring node qubits. Figures 3(c)–3(f) show the schematic diagram for the encoded measurement, which consists of three steps. First, we implement the Bell measurement between the two leaf qubits of neighboring hexagonal cluster states, as shown in Fig. 3(d). Then, we select the most reliable entanglement from the measurement results by comparing L likelihoods of the Bell measurements. The likelihoods are obtained from the measurement results as follows: We assume that the ith measurement deviations Δ_{m,A_i} and Δ_{m,B_i} are obtained from the ith Bell measurement on the two ith leaf qubits whose variance in the $q(p)$ quadrature is $\sigma^2_{\mathrm{leaf},q(p)}$. The ith likelihood is calculated by

$$F_i = f(\Delta_{m,A_i}) f(\Delta_{m,B_i}), \tag{26}$$

where $f(x)$ corresponds to the Gaussian distribution with mean zero and variance $\sigma^2_{\mathrm{leaf},q} + \sigma^2_{\mathrm{leaf},p} = 2\sigma^2$, i.e., the sum of the variances for the leaf qubit in the q and p quadratures.

Thirdly, we keep the most reliable entanglement while removing the remaining entanglement by comparing the m likelihoods. To keep the entanglement, we measure the ancillae connected to the most reliable entanglement in the q quadrature, as shown in Fig. 3(e). The probability of misidentifying the bit value in the q quadrature is sufficiently small compared to that in the p quadrature. For instance, the variance in the q quadrature is $\sigma^2/2$ or $2\sigma^2/5$, while the variance in the p quadrature is $2\sigma^2$ or $5\sigma^2/2$. As a result, we remove the ancillae from entanglement with a low error probability. For entanglement, except for the most reliable one, we perform the encoded measurement by measuring the ancillae in the p quadrature, as shown in Fig. 3(f). In the encoded measurement, we can obtain the bit value of the leaf qubit in the q quadrature by the m-repetition code. In the m-repetition code for the encoded leaf qubit, when there are no errors, the node qubit labeled by N and the ith ancilla labeled by A_i are stabilized by

$$\hat{Z}_N \hat{X}_{A_i} = +1 \, (i = 1, 2, \ldots, m), \tag{27}$$

where m corresponds to the number of ancilla qubits. After measuring the m ancilla qubits, we implement a majority vote among the measurement results of the ancillae in the p quadrature. As an example, we consider the case that the measurement results for the ancillae with $m = 3$ are $\hat{X}_{A_1} = +1$, $\hat{X}_{A_2} = +1$, and $\hat{X}_{A_3} = -1$, i.e., the bit values of the qubits A_1, A_2, and A_3 are measured as 0, 0, and 1, respectively. In this case, the bit value for the node qubit in the q quadrature is determined to be zero by a majority vote. This type of indirect measurement via ancilla qubits was introduced by Varnava *et al*. [78] for loss-tolerant optical quantum information processing. In our method, we apply the analog QEC [31] to the repetition code to enhance the QEC performance, where we compare two likelihoods for the logical bit values from the measurement results of the m ancilla qubits. The procedure for the m-repetition code with the analog QEC is described

in Ref. [31]. Consequently, we can obtain the large-scale 3D cluster state with a low error accumulation via the deterministic fusion gate with the encoded measurement.

IV. THRESHOLD CALCULATION

In this section, we numerically calculate the threshold of the squeezing level required for FTQC. In the numerical calculation, we simulate the QEC process for topologically protected MBQC by using the minimum-weight perfect-matching algorithm [79,80] for the code distances $d = 5$, 7, 9, and 11. In the simulation, we set the upper limit v_{up} for the HRM to $9\sqrt{\pi}/20$, and the number of ancilla qubits for the encoded measurement in the deterministic fusion gate is set to $m = 3$. In addition to the repetition code in the deterministic fusion gate, we apply the analog QEC [31] to decoding for the surface code in topologically protected MBQC to enhance the QEC performance. The procedure to apply the analog QEC to the surface code has been described in Ref. [32]. For an error model, we consider the errors derived from the variance for the node qubit itself, the accumulation of errors during the hexagonal cluster construction and deterministic fusion gate, assuming noise in the two-mode gate and homodyne measurement. For noise due to the two-mode gate described in Sec. II B, we assume that the squeezing level of the ancillary squeezed vacuum state is 15.0.

In Fig. 4, the logical error probabilities are plotted as a function of the standard deviation for photon loss in the homodyne measurement $l = 0$, 5, and 10%, where photon loss l is equal to $1 - \eta$ with a transmittance coefficient η described in Sec. II C. The numerical results confirm that our method for $l = 0$, 5, and 10% achieves the threshold values of the standard deviation, around 0.278, 0.234, and 0.168, which correspond to the threshold values of the squeezing level, around 8.1, 9.6, and 12.4 dB, respectively. The proposed scheme improves the threshold by about 2 dB compared to the previous one in Refs. [32,81]. Therefore, our scheme provides a high-threshold squeezing level for FTQC, even under noise in homodyne measurement and the two-mode gate.

V. DISCUSSION AND CONCLUSION

In this paper, we have developed a method to perform high-threshold FTQC with the GKP qubit under noise in the two-mode gate and homodyne measurement. In our method, we have proposed a maximum-likelihood method to reduce noise of the GKP qubits in the SQEC and the deterministic fusion gate with the encoded measurement, and combined the proposed methods with the conventional high-threshold FTQC [32]. The numerical calculations have shown that the required squeezing level can be improved to less than 10 dB with the analog QEC up to about a 5% transmission loss in the homodyne measurement, which could be generated with the near-term experimental setup. Furthermore, our method enables us to perform CV-FTQC with 12.4 dB for a 10% transmission loss, demonstrating numerically the robustness of CV-FTQC with GKP qubits against photon loss. In addition, there has been experimental progress in improving the squeezing level for CV quantum information processing, such as using squeezed light with an optical cavity [75,82,83] and waveguide devices [84–86]. Therefore, we believe that this paper will pave the way for CV-FTQC with a moderate squeezing level.

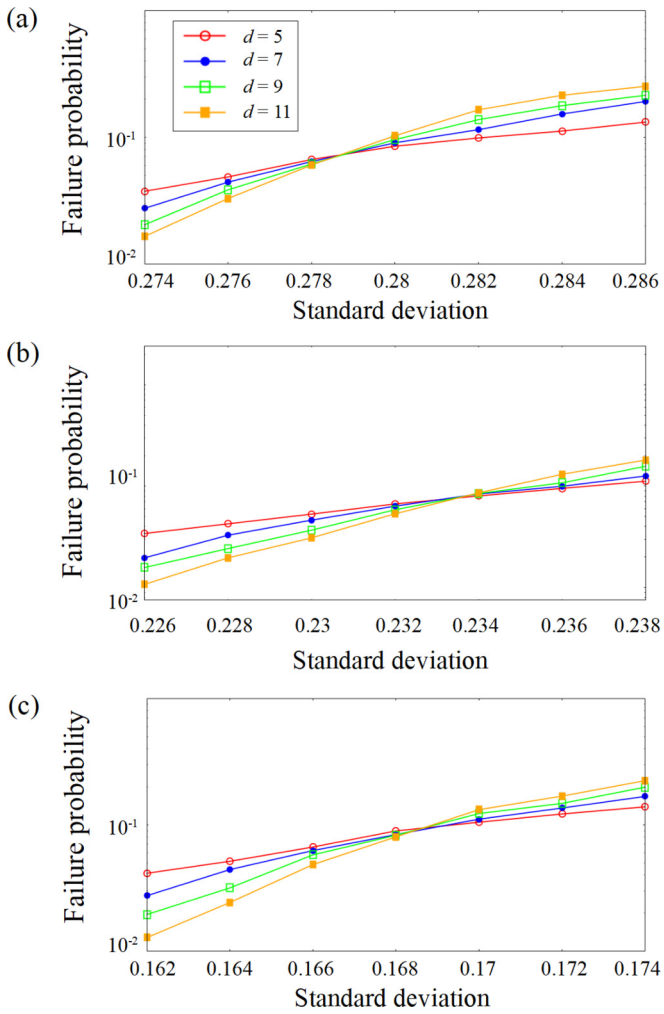

FIG. 4. Simulation results of the topologically protected MBQC with the analog QEC for the code distances $d = 5$, 7, 9, and 11. The failure probabilities of the QEC are plotted as a function of the standard deviation of the GKP qubits for loss in the homodyne measurement, (a) 0%, (b) 5%, and (c) 10%, respectively. The QEC process is simulated by using the 3D cluster prepared by the proposed method with $v_{\mathrm{up}} = 9\sqrt{\pi}/20$. The simulation results are obtained from 10 000 samples.

In future work, we will analyze the resources required for CV-FTQC, such as the number of qubits needed to implement a quantum algorithm at various squeezing levels. Additionally, we could apply the proposed scheme to noise that includes imperfections during the generation of the GKP qubit. Such a noise model has been studied in Refs. [33,36].

ACKNOWLEDGMENTS

K.F. thanks Keisuke Fujii for useful discussions. This work was partly supported by Japan Science and Technology Agency (Moonshot R&D) Grants No. JPMJMS2064 and No. JPMJMS2061, the University of Tokyo Foundation, and donations from Nichia Corporation.

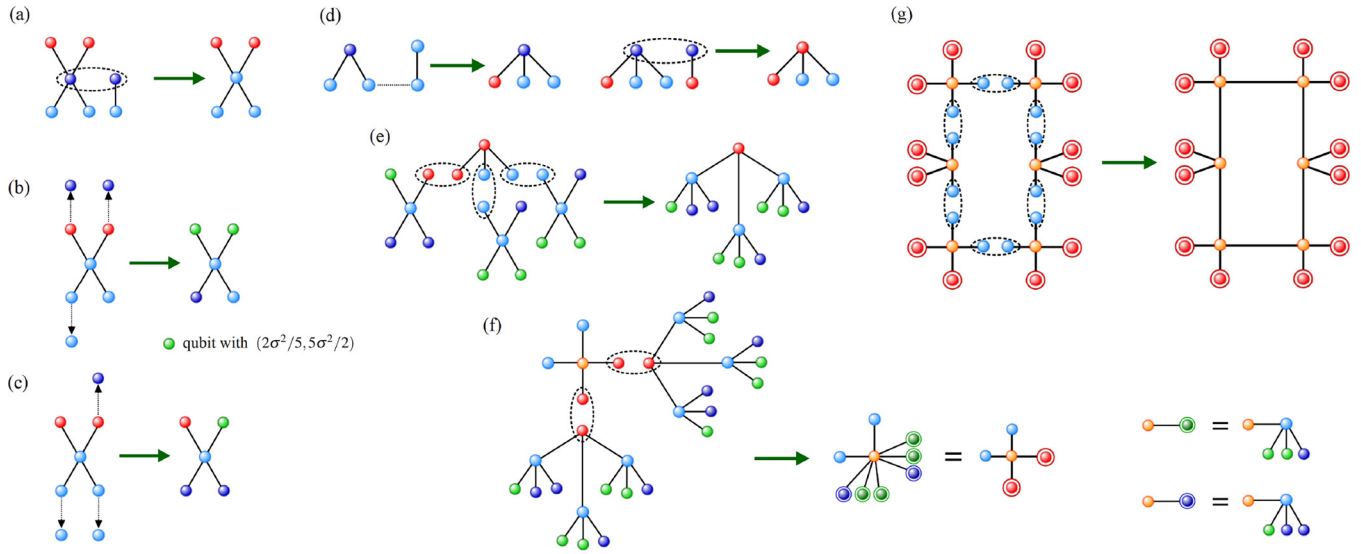

FIG. 5. The construction of the encoded hexagonal cluster state via fusion gates with the HRM. (a)–(c) The construction of three types of the five-tree cluster state. (d) The construction of the four-tree cluster state. (e) The construction of the encoded leaf qubit from the four-tree cluster state and the five-tree cluster states. (f) The construction of the encoded five-tree cluster state consisting of three qubits and two encoded qubits. Each encoded qubit consists of the $L = 3$ encoded leaf qubits. Each encoded leaf qubit consists of the $m + 1 = 4$ qubits used for the m-repetition code. (g) The construction of the encoded hexagonal cluster with the encoded leaf qubits from the six encoded five-tree cluster states.

APPENDIX A: SINGLE-QUBIT LEVEL QEC IN THE *p* QUADRATURE

We describe the SQEC in the p quadrature after the SQEC in the q quadrature. The SQEC in the p quadrature is performed using the additional ancilla qubit A_2 prepared in the state $|\widetilde{+}\rangle_{A_2} = (|\widetilde{0}\rangle_{A_2} + |\widetilde{1}\rangle_{A_2})/\sqrt{2}$. The data qubit D is interacted with the ancilla A_2 by the CX gate, where the ancilla qubit is assumed to be the control qubit. Regarding the deviation, the CX gate operation transforms the deviations in the q and p quadratures as

$$\overline{\Delta}_{q,a_2} \to \overline{\Delta}_{q,a_2}, \tag{A1}$$

$$\overline{\Delta}_{p,a_2} \to \overline{\Delta}_{p,a_2} - \overline{\Delta}_{p,D} + \overline{\Delta}_{p,a}, \tag{A2}$$

$$-\overline{\Delta}_{q,a} \to -\overline{\Delta}_{q,a} + \overline{\Delta}_{q,a_2}, \tag{A3}$$

$$\overline{\Delta}_{p,D} - \overline{\Delta}_{p,a} \to \overline{\Delta}_{p,D} - \overline{\Delta}_{p,a}, \tag{A4}$$

where $\overline{\Delta}_{q,a2}(\overline{\Delta}_{p,a2})$ is the true deviation value of the ancilla A_2 in the q (p) quadrature. Then we measure the ancilla in the p quadrature, and obtain the deviation of the ancilla Δ_{mp,a_2}. Then we measure the ancilla qubit in the p quadrature, and obtain the measurement outcome $m_{p,m} = (2t + k)\sqrt{\pi} + \Delta_{mp,a_2}$ to minimize $|\Delta_{mp,a_2}|$, where k is the bit value and $t = 0, \pm 1, \pm 2, \ldots$. If $|\Delta_{mp,a2}| = |\overline{\Delta}_{q,a2} - \overline{\Delta}_{q,D} + \overline{\Delta}_{p,a}|$ is less than $\sqrt{\pi}/2$, the true deviation value of the data qubit in the q quadrature changes from $\overline{\Delta}_{q,D} - \overline{\Delta}_{q,a}$ to $\overline{\Delta}_{q,a2}$ after the displacement operation. If $|\Delta_{mq,a2}|$ is more than $\sqrt{\pi}/2$, the phase-flip error occurs after the displacement operation. Consequently, the sequential SQECs in the q and p quadratures transform the variances of the data qubit in the q and p quadratures as $\sigma^2_{D,q} \to \sigma^2_{a,q} + \sigma^2_{a_2,q}$ and $\sigma^2_{D,p} \to \sigma^2_{a_2,p}$, respectively. In this paper, we employ the ME-SQEC to reduce the variances, as described in Sec. II E.

APPENDIX B: CONSTRUCTION OF THE HEXAGONAL CLUSTER STATE

We describe the construction of the encoded hexagonal cluster state from the cluster states described in Fig. 2, where larger-scale cluster states are generated from smaller-scale cluster states by using the fusion gate with the HRM, as depicted in Fig. 5. We describe the preparation of the encoded hexagonal cluster state, where each node qubit consists of $2L = 6$ encoded leaf qubits and each encoded leaf qubit consists of $m = 3$ ancilla qubits. We note that the fusion gate does not increase the variances of the node qubits, and the HRM is used to ensure reliability for the fusion gate until the encoded hexagonal cluster state is prepared. During the construction of the encoded hexagonal cluster state, the error probabilities of the measurements are limited to at most $E_{v_{\rm up}}(5\sigma^2/2)$ for each measurement.

Figures 5(a)–5(c) show the construction of three types of the five-tree cluster states. For the five-tree cluster state in Fig. 5(a), the cluster state is prepared by the fusion gate between the qubits of cluster states in Figs. 2(b) and 2(g), where the error probability in the fusion gate is given by $E_{v_{\rm up}}(5\sigma^2/2)$. Figure 5(b) describes the five-tree cluster state via the three ME-SQECs in the q quadrature on the qubits in Fig. 5(a), where the error probabilities in the ME-SQECs are given by $E_{v_{\rm up}}(2\sigma^2)$ and $E_{v_{\rm up}}(5\sigma^2/2)$. The ME-SQECs in the q quadrature transform variances as $(2\sigma^2, \sigma^2/2) \mapsto (2\sigma^2/5, 5\sigma^2/2)$ and $(\sigma^2, \sigma^2) \mapsto (\sigma^2/2, 2\sigma^2)$. Figure 5(c) describes the five-tree cluster state via the three ME-SQECs in the q quadrature on the qubit in the five-tree cluster state in Fig. 5(b). Figure 5(d) describes the four-tree cluster state. For this four-tree cluster state, we first prepare the four-tree cluster state with the node qubit whose variance is $(\sigma^2/2, 2\sigma^2)$, where we perform the CZ gate between the qubits in the

three-tree cluster state and the balanced-entangled pair, and implement the Fourier transformation after the measurement. Then, we apply the fusion gate between the qubits in the four-tree cluster state and the biased-entangled pair to obtain the four-tree cluster state with the node qubit whose variance is $(2\sigma^2, \sigma^2/2)$, where the error probability in the fusion gate is given by $E_{v_{\rm up}}(5\sigma^2/2)$. Figure 5(e) describes the construction of the encoded leaf qubit from the four-tree cluster state and the five-tree cluster state by using the fusion gates. Figure 5(f) describes the construction of the encoded five-tree cluster state via the fusion gate between the qubits in the cluster states in Figs. 5(d) and 5(e). The encoded five-tree cluster state, i.e., the encoded leaf qubit, consists of the $2L$ encoded ancilla qubits, where each encoded ancilla qubit consists of the single leaf qubit and three ancilla qubits. These ancilla qubits are used for the encoded measurement to realize the reliable entanglement generation between the node qubits in the neighboring hexagonal cluster states, as described in Sec. III B. Finally, the encoded hexagonal cluster state is constructed from the six encoded five-tree cluster states, as shown in Fig. 5(g). For the error probabilities, the probability of errors in the fusion gate between qubits with variances of (σ^2, σ^2) is given by $E_{v_{\rm up}}(2\sigma^2)$, while that between qubits between variances of $(\sigma^2/2, 2\sigma^2)$ is $E_{v_{\rm up}}(5\sigma^2/2)$. Accordingly, the error probabilities of the fusion gate are limited to $E_{v_{\rm up}}(5\sigma^2/2)$ at most during the preparation of the encoded hexagonal cluster state. In the construction of the hexagonal cluster state, the maximum error probability for the proposed scheme, $E_{v_{\rm up}}(5\sigma^2/2)$, is improved compared to the scheme in Ref. [32], $E_{v_{\rm up}}(3\sigma^2)$. Thus, we obtain the highly reliable encoded hexagonal cluster state with low error accumulation at the cost of the success probability for the HRM. This method is used for the deterministic generation of a large-scale cluster state required for CV-FTQC.

[1] P. W. Shor, Polynomial-time algorithms for prime factorization and discrete logarithms on a quantum computer, SIAM Rev. **41**, 303 (1999).

[2] L. K. Grover, Quantum Mechanics Helps in Searching for a Needle in a Haystack, Phys. Rev. Lett. **79**, 325 (1997).

[3] S. Takeda and A. Furusawa, Toward large-scale fault-tolerant universal photonic quantum computing, APL Photonics **4**, 060902 (2019).

[4] O. Pfister, Continuous-variable quantum computing in the quantum optical frequency comb, J. Phys. B **53**, 012001 (2020).

[5] K. Fukui and S. Takeda, Building a large-scale quantum computer with continuous-variable optical technologies, J. Phys. B **55**, 012001 (2022).

[6] S. Yokoyama, R. Ukai, S. C. Armstrong, C. Sornphiphatphong, T. Kaji, S. Suzuki, J. Yoshikawa, H. Yonezawa, N. C. Menicucci, and A. Furusawa, Ultra-large-scale continuous-variable cluster states multiplexed in the time domain, Nat. Photon. **7**, 982 (2013).

[7] J. Yoshikawa, S. Yokoyama, T. Kaji, C. Sornphiphatphong, Y. Shiozawa, K. Makino, and A. Furusawa, Invited article: Generation of one-million-mode continuous-variable cluster state by unlimited time-domain multiplexing, APL Photonics **1**, 060801 (2016).

[8] W. Asavanant, Y. Shiozawa, S. Yokoyama, B. Charoensombutamon, H. Emura, R. N. Alexander, S. Takeda, J. Yoshikawa, N. C. Menicucci, H. Yonezawa *et al.*, Generation of time-domain-multiplexed two-dimensional cluster state, Science **366**, 373 (2019).

[9] M. V. Larsen, X. Guo, C. R. Breum, J. S. Neergaard-Nielsen, and U. L. Andersen, Deterministic generation of a two-dimensional cluster state, Science **366**, 369 (2019).

[10] M. V. Larsen, X. Guo, C. R. Breum, J. S. Neergaard-Nielsen, and U. L. Andersen, Deterministic multi-mode gates on a scalable photonic quantum computing platform, Nat. Phys. **17**, 1018 (2021).

[11] W. Asavanant, B. Charoensombutamon, S. Yokoyama, T. Ebihara, T. Nakamura, R. N. Alexander, M. Endo, J. Yoshikawa, N. C. Menicucci, H. Yonezawa *et al.*, Time-Domain-Multiplexed Measurement-Based Quantum Operations with 25-MHz Clock Frequency, Phys. Rev. Applied **16**, 034005 (2021).

[12] M. Pysher, Y. Miwa, R. Shahrokhshahi, R. Bloomer, and O. Pfister, Parallel Generation of Quadripartite Cluster Entanglement in the Optical Frequency Comb, Phys. Rev. Lett. **107**, 030505 (2011).

[13] M. Chen, N. C. Menicucci, and O. Pfister, Experimental Realization of Multipartite Entanglement of 60 Modes of a Quantum Optical Frequency Comb, Phys. Rev. Lett. **112**, 120505 (2014).

[14] J. Roslund, R. M. De Araujo, S. Jiang, C. Fabre, and N. Treps, Wavelength-multiplexed quantum networks with ultrafast frequency combs, Nat. Photon. **8**, 109 (2014).

[15] Y. Cai, J. Roslund, G. Ferrini, F. Arzani, X. Xu, C. Fabre, and N. Treps, Multimode entanglement in reconfigurable graph states using optical frequency combs, Nat. Commun. **8**, 15645 (2017).

[16] A. L. Grimsmo and A. Blais, Squeezing and quantum state engineering with Josephson travelling wave amplifiers, npj Quantum Inf. **3**, 20 (2017).

[17] M. Schmidt, M. Ludwig, and F. Marquardt, Optomechanical circuits for nanomechanical continuous variable quantum state processing, New J. Phys. **14**, 125005 (2012).

[18] O. Houhou, H. Aissaoui, and A. Ferraro, Generation of cluster states in optomechanical quantum systems, Phys. Rev. A **92**, 063843 (2015).

[19] Y. Ikeda and N. Yamamoto, Deterministic generation of gaussian pure states in a quasilocal dissipative system, Phys. Rev. A **87**, 033802 (2013).

[20] K. R. Motes, B. Q. Baragiola, A. Gilchrist, and N. C. Menicucci, Encoding qubits into oscillators with atomic ensembles and squeezed light, Phys. Rev. A **95**, 053819 (2017).

[21] C. Flühmann, V. Negnevitsky, M. Marinelli, and J. P. Home, Sequential Modular Position and Momentum Measurements of a Trapped Ion Mechanical Oscillator, Phys. Rev. X **8**, 021001 (2018).

[22] C. Flühmann, T. L. Nguyen, M. Marinelli, V. Negnevitsky, K. Mehta, and J. Home, Encoding a qubit in a trapped-ion mechanical oscillator, Nature (London) **566**, 513 (2019).

[23] D. T. Pegg and S. M. Barnett, Phase properties of the quantized single-mode electromagnetic field, Phys. Rev. A **39**, 1665 (1989).
[24] I. L. Chuang, D. W. Leung, and Y. Yamamoto, Bosonic quantum codes for amplitude damping, Phys. Rev. A **56**, 1114 (1997).
[25] V. V. Albert, K. Noh, K. Duivenvoorden, D. J. Young, R. T. Brierley, P. Reinhold, C. Vuillot, L. Li, C. Shen, S. M. Girvin, B. M. Terhal, and L. Jiang, Performance and structure of single-mode bosonic codes, Phys. Rev. A **97**, 032346 (2018).
[26] A. L. Grimsmo, J. Combes, and B. Q. Baragiola, Quantum Computing with Rotation-Symmetric Bosonic Codes, Phys. Rev. X **10**, 011058 (2020).
[27] P. T. Cochrane, G. J. Milburn, and W. J. Munro, Macroscopically distinct quantum-superposition states as a bosonic code for amplitude damping, Phys. Rev. A **59**, 2631 (1999).
[28] M. H. Michael, M. Silveri, R. T. Brierley, V. V. Albert, J. Salmilehto, L. Jiang, and S. M. Girvin, New Class of Quantum Error-Correcting Codes for a Bosonic Mode, Phys. Rev. X **6**, 031006 (2016).
[29] D. Gottesman, A. Kitaev, and J. Preskill, Encoding a qubit in an oscillator, Phys. Rev. A **64**, 012310 (2001).
[30] N. C. Menicucci, Fault-Tolerant Measurement-Based Quantum Computing with Continuous-Variable Cluster States, Phys. Rev. Lett. **112**, 120504 (2014).
[31] K. Fukui, A. Tomita, and A. Okamoto, Analog Quantum Error Correction with Encoding a Qubit into an Oscillator, Phys. Rev. Lett. **119**, 180507 (2017).
[32] K. Fukui, A. Tomita, A. Okamoto, and K. Fujii, High-Threshold Fault-Tolerant Quantum Computation with Analog Quantum Error Correction, Phys. Rev. X **8**, 021054 (2018).
[33] T. Douce, D. Markham, E. Kashefi, P. Van Loock, and G. Ferrini, Probabilistic fault-tolerant universal quantum computation and sampling problems in continuous variables, Phys. Rev. A **99**, 012344 (2019).
[34] C. Vuillot, H. Asasi, Y. Wang, L. P. Pryadko, and B. M. Terhal, Quantum error correction with the toric Gottesman-Kitaev-Preskill code, Phys. Rev. A **99**, 032344 (2019).
[35] B. Q. Baragiola, G. Pantaleoni, R. N. Alexander, A. Karanjai, and N. C. Menicucci, All-Gaussian Universality and Fault Tolerance with the Gottesman-Kitaev-Preskill Code, Phys. Rev. Lett. **123**, 200502 (2019).
[36] Y. Shi, C. Chamberland, and A. Cross, Fault-tolerant preparation of approximate GKP states, New J. Phys. **21**, 093007 (2019).
[37] B. W. Walshe, L. J. Mensen, B. Q. Baragiola, and N. C. Menicucci, Robust fault tolerance for continuous-variable cluster states with excess antisqueezing, Phys. Rev. A **100**, 010301(R) (2019).
[38] G. Pantaleoni, B. Q. Baragiola, and N. C. Menicucci, Modular Bosonic Subsystem Codes, Phys. Rev. Lett. **125**, 040501 (2020).
[39] B. W. Walshe, B. Q. Baragiola, R. N. Alexander, and N. C. Menicucci, Continuous-variable gate teleportation and bosonic-code error correction, Phys. Rev. A **102**, 062411 (2020).
[40] G. Pantaleoni, B. Q. Baragiola, and N. C. Menicucci, Subsystem analysis of continuous-variable resource states, Phys. Rev. A **104**, 012430 (2021).
[41] A. L. Grimsmo and S. Puri, Quantum error correction with the Gottesman-Kitaev-Preskill code, PRX Quantum **2**, 020101 (2021).
[42] K. Fukui, A. Tomita, and A. Okamoto, Tracking quantum error correction, Phys. Rev. A **98**, 022326 (2018).
[43] K. Noh and C. Chamberland, Fault-tolerant bosonic quantum error correction with the surface–Gottesman-Kitaev-Preskill code, Phys. Rev. A **101**, 012316 (2020).
[44] K. Noh, S. M. Girvin, and L. Jiang, Encoding an Oscillator into Many Oscillators, Phys. Rev. Lett. **125**, 080503 (2020).
[45] H. Yamasaki, K. Fukui, Y. Takeuchi, S. Tani, and M. Koashi, Polylog-overhead highly fault-tolerant measurement-based quantum computation: All-gaussian implementation with Gottesman-Kitaev-Preskill code, arXiv:2006.05416.
[46] I. Tzitrin, T. Matsuura, R. N. Alexander, G. Dauphinais, J. E. Bourassa, K. K. Sabapathy, N. C. Menicucci, and I. Dhand, Fault-tolerant quantum computation with static linear optics, PRX Quantum **2**, 040353 (2021).
[47] K. Noh, C. Chamberland, and F. G. Brandão, Low-overhead fault-tolerant quantum error correction with the surface-GKP code, PRX Quantum **3**, 010315 (2022).
[48] K. P. Seshadreesan, P. Dhara, A. Patil, L. Jiang, and S. Guha, Coherent manipulation of graph states composed of finite-energy Gottesman-Kitaev-Preskill-encoded qubits, Phys. Rev. A **105**, 052416 (2022).
[49] K. Fukui and N. C. Menicucci, An efficient, concatenated, bosonic code for additive Gaussian noise, arXiv:2102.01374.
[50] M. P. Stafford and N. C. Menicucci, Biased Gottesman-Kitaev-Preskill repetition code, arXiv:2212.11397.
[51] S. Takeda and A. Furusawa, Universal Quantum Computing with Measurement-Induced Continuous-Variable Gate Sequence in a Loop-Based Architecture, Phys. Rev. Lett. **119**, 120504 (2017).
[52] R. N. Alexander, S. Yokoyama, A. Furusawa, and N. C. Menicucci, Universal quantum computation with temporal-mode bilayer square lattices, Phys. Rev. A **97**, 032302 (2018).
[53] J. E. Bourassa, R. N. Alexander, M. Vasmer, A. Patil, I. Tzitrin, T. Matsuura, D. Su, B. Q. Baragiola, S. Guha, G. Dauphinais *et al.*, Blueprint for a scalable photonic fault-tolerant quantum computer, Quantum **5**, 392 (2021).
[54] K. Fukui, R. N. Alexander, and P. van Loock, All-optical long-distance quantum communication with Gottesman-Kitaev-Preskill qubits, Phys. Rev. Res. **3**, 033118 (2021).
[55] F. Rozpędek, K. Noh, Q. Xu, S. Guha, and L. Jiang, Quantum repeaters based on concatenated bosonic and discrete-variable quantum codes, npj Quantum Inf. **7**, 102 (2021).
[56] B. M. Terhal and D. Weigand, Encoding a qubit into a cavity mode in circuit QED using phase estimation, Phys. Rev. A **93**, 012315 (2016).
[57] P. Campagne-Ibarcq, A. Eickbusch, S. Touzard, E. Zalys-Geller, N. E. Frattini, V. V. Sivak, P. Reinhold, S. Puri, S. Shankar, R. J. Schoelkopf *et al.*, Quantum error correction of a qubit encoded in grid states of an oscillator, Nature **584**, 368 (2020).
[58] S. Pirandola, S. Mancini, D. Vitali, and P. Tombesi, Constructing finite-dimensional codes with optical continuous variables, Europhys. Lett. **68**, 323 (2004).
[59] S. Pirandola, S. Mancini, D. Vitali, and P. Tombesi, Continuous variable encoding by ponderomotive interaction, European Phys. J. D: Atomic, Molecular, Optical Plasma Phys. **37**, 283 (2006).
[60] S. Pirandola, S. Mancini, D. Vitali, and P. Tombesi, Generating continuous variable quantum codewords in

the near-field atomic lithography, J. Phys. B **39**, 997 (2006).

[61] M. Eaton, R. Nehra, and O. Pfister, Non-Gaussian and Gottesman-Kitaev-Preskill state preparation by photon catalysis, New J. Phys. **21**, 113034 (2019).

[62] D. Su, C. R. Myers, and K. K. Sabapathy, Conversion of gaussian states to non-gaussian states using photon-number-resolving detectors, Phys. Rev. A **100**, 052301 (2019).

[63] J. M. Arrazola, T. R. Bromley, J. Izaac, C. R. Myers, K. Brádler, and N. Killoran, Machine learning method for state preparation and gate synthesis on photonic quantum computers, Quantum Sci. Technol. **4**, 024004 (2019).

[64] I. Tzitrin, J. E. Bourassa, N. C. Menicucci, and K. K. Sabapathy, Progress towards practical qubit computation using approximate Gottesman-Kitaev-Preskill codes, Phys. Rev. A **101**, 032315 (2020).

[65] C.-Y. Lin, W.-C. Su, and S.-T. Wu, Encoding qubits into harmonic-oscillator modes via quantum walks in phase space, Quant. Info. Proc. **19**, 272 (2020).

[66] J. Hastrup and U. L. Andersen, Protocol for Generating Optical Gottesman-Kitaev-Preskill States with Cavity QED, Phys. Rev. Lett. **128**, 170503 (2022).

[67] K. Fukui, M. Endo, W. Asavanant, A. Sakaguchi, J. Yoshikawa, and A. Furusawa, Generating the Gottesman-Kitaev-Preskill qubit using a cross-Kerr interaction between squeezed light and Fock states in optics, Phys. Rev. A **105**, 022436 (2022).

[68] K. Takase, K. Fukui, A. Kawasaki, W. Asavanant, M. Endo, J. Yoshikawa, P. van Loock, and A. Furusawa, Gaussian breeding for encoding a qubit in propagating light, arXiv:2212.05436.

[69] R. Yanagimoto, R. Nehra, R. Hamerly, E. Ng, A. Marandi, and H. Mabuchi, Quantum nondemolition measurements with optical parametric amplifiers for ultrafast universal quantum information processing, PRX Quantum **4**, 010333 (2023).

[70] We have considered only noise from loss in the homodyne measurement and the two-mode gate, while there are other noises such as nonlinear errors, thermal noise, and so on. The threshold including such errors remains an open problem.

[71] We note that the $q(p)$ quadrature is also referred to as the $Z(X)$ basis to consider the GKP qubit as equivalent to the qubit for discrete variables in this paper.

[72] K. Duivenvoorden, B. M. Terhal, and D. Weigand, Single-mode displacement sensor, Phys. Rev. A **95**, 012305 (2017).

[73] J. Yoshikawa, Y. Miwa, A. Huck, U. L. Andersen, P. Van Loock, and A. Furusawa, Demonstration of a Quantum Nondemolition Sum Gate, Phys. Rev. Lett. **101**, 250501 (2008).

[74] Y. Shiozawa, J. Yoshikawa, S. Yokoyama, T. Kaji, K. Makino, T. Serikawa, R. Nakamura, S. Suzuki, S. Yamazaki, W. Asavanant, S. Takeda, P. van Loock, and A. Furusawa, Quantum nondemolition gate operations and measurements in real time on fluctuating signals, Phys. Rev. A **98**, 052311 (2018).

[75] H. Vahlbruch, M. Mehmet, K. Danzmann, and R. Schnabel, Detection of 15 dB Squeezed States of Light and their Application for the Absolute Calibration of Photoelectric Quantum Efficiency, Phys. Rev. Lett. **117**, 110801 (2016).

[76] D. Harville, Extension of the Gauss-Markov theorem to include the estimation of random effects, Ann. Stat. **4**, 384 (1976).

[77] We note that we could use the ME-SQEC several times to reduce the variances when we prepare the cluster state from the GKP qubits, as described in arXiv:1906.09767 v1. In the case of the cluster state prepared from the qunaught states, it is sufficient to use the ME-SQEC only once since the variances are sufficiently small.

[78] M. Varnava, D. E. Browne, and T. Rudolph, Loss Tolerance in One-Way Quantum Computation via Counterfactual Error Correction, Phys. Rev. Lett. **97**, 120501 (2006).

[79] J. Edmonds, Paths, trees, and flowers, Can. J. Math. **17**, 449 (1965).

[80] V. Kolmogorov, Blossom V: A new implementation of a minimum cost perfect matching algorithm, Mathematical Programming Computation **1**, 43 (2009).

[81] In addition, we simulated the QEC in the case where squeezing for ancillary squeezed vacuum states in the two-mode gate is infinite, and loss in the homodyne measurement is zero. In that case, we obtained the threshold of the standard deviation ≈ 0.287, which corresponds to ≈ 7.8 dB.

[82] S. Suzuki, H. Yonezawa, F. Kannari, M. Sasaki, and A. Furusawa, 7 dB quadrature squeezing at 860 nm with periodically poled K Ti OPO_4, Appl. Phys. Lett. **89**, 061116 (2006).

[83] K. Nagashima, G. Masada, H. Arao, Y. Takeno, H. Yonezawa, and A. Furusawa, Generation of highly squeezed light at 860 nm, in *2008 International Nano-Optoelectronics Workshop* (IEEE, New York, 2008), pp. 165–166.

[84] T. Kashiwazaki, N. Takanashi, T. Yamashima, T. Kazama, K. Enbutsu, R. Kasahara, T. Umeki, and A. Furusawa, Continuous-wave 6-db-squeezed light with 2.5-THz-bandwidth from single-mode PPLN waveguide, APL Photonics **5**, 036104 (2020).

[85] T. Kashiwazaki, T. Yamashima, N. Takanashi, A. Inoue, T. Umeki, and A. Furusawa, Fabrication of low-loss quasi-single-mode PPLN waveguide and its application to a modularized broadband high-level squeezer, Appl. Phys. Lett. **119**, 251104 (2021).

[86] T. Kashiwazaki, T. Yamashima, K. Enbutsu, T. Kazama, A. Inoue, K. Fukui, M. Endo, T. Umeki, and A. Furusawa, Over-8-db squeezed light generation by a broadband waveguide optical parametric amplifier toward fault-tolerant ultra-fast quantum computers, arXiv:2301.12658.